THE JOURNAL OF BIOLOGICAL CHEMISTRY
Vol. 280, No. 30242, Issue of August 26, pp. 30242–30253, 2005
Printed in U.S.A.

Cleavage of p21/WAF1/CIP1 by Proteinase 3 Modulates Differentiation of a Monocytic Cell Line

MOLECULAR ANALYSIS OF THE CLEAVAGE SITE*

Received for publication, December 27, 2004, and in revised form, June 9, 2005
Published, JBC Papers in Press, June 23, 2005, DOI 10.1074/jbc.M414609200

Bernard Dublet‡§, Antonella Ruello¶§, Magali Pederzoli¶, Eric Hajjar‖, Marie Courbebaisse¶, Sandrine Canteloup¶, Nathalie Reuter‖, and Véronique Witko-Sarsat¶**

From the ‡Laboratoire de Spectrométrie de Masse des Protéines, Institut de Biologie Structurale Jean-Pierre Ebel, Commissariat à l'Energie Atomique-CNRS-Université Joseph Fourier, Grenoble 38000, France, ‖Computational Biology Unit, Bergen Center for Computational Science, University of Bergen, Bergen 5020, Norway, and ¶INSERM U507, Université René Descartes Paris 5, Hôpital Necker, 161 rue de Sèvres, Paris 75015, France

Proteinase 3 (PR3), also called myeloblastin, is involved in the control of myeloid cell growth, but the underlying molecular mechanisms have not been elucidated. In U937/PR3, stably transfected with PRCRSV/PR3 to overexpress PR3, PMA-induced p21 expression was significantly decreased as compared with control U937, and this phenomenon was reversed in the presence of the serine proteinase inhibitor, pefabloc. Conversely, when PR3 was inactivated by small interfering RNA, p21 protein was increased, and PMA-induced monocytic differentiation was potentiated. Mass spectrometry analysis identified Ala^{45} as the primary cleavage site on p21, and the recombinant mutated p21A45R, generated by site-directed mutagenesis and expressed in *Escherichia coli*, was resistant to *in vitro* PR3 cleavage. The U937 cells were then stably transfected with either PRCRSV/p21 or PRCRSV/p21A45R, to ectopically express wild type p21 or PR3-resistant p21, respectively. In U937/p21A45R treated with PS-341, a selective proteasome inhibitor, a significant decrease in the S phase and a blockade in the G_0-G_1 phase of cell cycle were observed when compared with U937/p21 or control U937. This suggested that both PR3 and the proteasome are efficiently involved in the proteolytic regulation of p21 expression in myeloid cells. Moreover, PMA-induced p21 expression was more pronounced in U937/p21A45R compared with U937/p21 and was concomitant with the morphological features of early differentiation. Our data demonstrated that p21 is one specific target of PR3 and that PR3-mediated p21 cleavage prevents monocytic differentiation.

Proteinase 3 (PR3)[1] is a neutrophil-derived proteinase originally described in azurophilic granules along with its homologues elastase, cathepsin G, and azurocidin (1–3). Despite the strong homology between PR3 and elastase, PR3 appears to display some functional and structural features of its own (4, 5). Interestingly, PR3 was cloned in HL-60 myeloid cells and was called myeloblastin, because its mRNA was down-regulated during myeloid differentiation (6). PR3 has been involved in the control of proliferation in normal hematopoietic progenitors and in early steps in their transformation. PR3 is overexpressed in myeloid leukemia (7, 8). Further studies have shown that PR3 is a granulocyte-macrophage colony-stimulating factor-responsive gene, which can confer serum independence to precursor cells (9). Although several molecular targets have been postulated, such as the transcription factor Sp1 (10) or the 28-kDa heat shock protein (11), no clear demonstration has identified a specific PR3 target involved in the regulation of proliferation. In a model of mast cell lines (RBL and HMC1) stably transfected with either PR3 or elastase or an inactive PR3 mutant PR3S203A, we have provided evidence that PR3, but not elastase or its inactive mutant PR3S203A, had a proliferative activity and that the cyclin-dependent kinase inhibitor p21/WAF1/CIP1 was a molecular target of PR3 (12). p21 belongs to the family of cyclin-dependent kinase inhibitors (13). It inhibits cyclin-dependent kinase-1, -2, -4, and -6 (14), and its induction by a number of stimuli including p53 (15) induces cell cycle arrest at the G_1/S boundary, allowing the cell to exit the cell cycle and differentiate (16). In several hematopoietic cell lines, including U937, the p21 gene is a primary response gene tightly related to early markers of the differentiation program (17). Likewise, myeloid maturation of CD34+ precursor cells is associated with a marked increase in p21 expression (18). The concomitant expression of both PR3 and p21 during the early phase of myeloid cell differentiation raised the possibility that these key proteins may regulate each other, leading to a coordinated process of differentiation.

In the present study, we first performed a molecular analysis of the cleavage site on p21 by PR3 in order to generate p21A45R, a PR3-resistant p21. We next addressed the question of the physiological relevance of the p21 cleavage by PR3 in myeloid cells expressing endogenous PR3. The construction of genetically modified U937 cells, which expressed endogenous PR3 (19), made it possible to study (i) the effect of an overexpression of PR3 in U937/PR3 and (ii) the effect of the inactivation of PR3 using siRNA or (iii) the effect of the expression of PR3-resistant p21, thereby enabling us to address the role of PR3 in monocytic

* This work was supported by FUGE (Norwegian Functional Genomics Program) through the technology platform for bioinformatics (to N. R. and E. H.) and by EGIDE (to N. R. and V. W.-S.). This work was also supported by the Association "Vaincre la Mucoviscidose," "Association pour la Recherche sur la Polyarthrite" (to ARP) (fellowship to M. P.), and the "Leg Poix" (to V. W.-S.). This work was also supported by BAXTER (Extramural Grant to V. W.-S.) and AMGEN. The costs of publication of this article were defrayed in part by the payment of page charges. This article must therefore be hereby marked "*advertisement*" in accordance with 18 U.S.C. Section 1734 solely to indicate this fact.

§ These two authors contributed equally to this work.

** To whom correspondence should be addressed: INSERM U507, Hôpital Necker, 161 Rue de Sèvres, Paris 75015, France. Tel.: 33-01-44-38-16-03; Fax: 33-01-45-66-51-33; E-mail: witko-sarsat@necker.fr.

[1] The abbreviations used are: PR3, proteinase 3; FCS, fetal calf serum; MALDI-TOF, matrix-assisted laser desorption ionization time-of-flight; MD, molecular dynamics; PBS, phosphate-buffered saline; PMA, phorbol myristate acetate; siRNA, small interfering RNA; aa, amino acids; RT, reverse transcription.

differentiation. We herein provide evidence that overexpression of PR3 in the promonocytic cell line U937 enhanced p21 cleavage and that inhibition of PR3 activity either by small interfering RNA or by ectopic expression of the p21A45R potentiated the early steps of monocytic differentiation.

EXPERIMENTAL PROCEDURES

cDNA and the Construction of Expression Vectors

PR3 cDNA from pCDNA3/PR3 was subcloned into the expression vector PRC/RSV/PR3 (Invitrogen) between HindIII and NotI restriction sites (12). The plasmid pETp21/His containing the human p21 cDNA with an N-terminal His tag was a gift from Dr. Bruce Stillman (Cold Spring Harbor, NY) (20). The plasmid PRC/RSV/p21 was obtained by subcloning p21 cDNA from pETp21/His into the XbaI restriction site. The plasmid PRC/RSV/p21A52R was prepared to express the PR3-resistant p21 by mutating the alanine residue (Ala^{45}) into arginine (Arg^{45}) using the following primers: forward, GCT GCA TCC AGG AGC GCC GTG AGC GAT GG; reverse, CCA TCG CTC ACG GCG CTC CTG GAT GCA GC. Mutagenesis was performed using the QuikChange method according to the manufacturer's instructions (Clontech). All cDNA sequences were confirmed by direct sequencing (data not shown).

Enzymatic Cleavage of Recombinant p21 by Neutrophil PR3

Recombinant human p21 was purified from *Escherichia coli* transformed with the expression plasmid pETp21/His expressing a His tag at the N terminus (20). Recombinant p21 protein was purified under denaturing conditions. Briefly, growing bacteria were induced by isopropyl 1-thio-β-D-galactopyranoside for 15 h at 30 °C, centrifuged, and lysed in a denaturing buffer (100 mM NaH_2PO_4, 10 mM Tris, 8 M urea, pH 8.0). The supernatant was loaded onto a Ni^{2+}-nitrilotriacetic acid column, and the p21 was eluted by a pH gradient (100 mM NaH_2PO_4, 10 mM Tris, 8 M urea, pH 5.9 to 4.5). The presence of p21 was tested by Western blot, and the p21-positive fractions were pooled and dialyzed in 10 mM Tris, 50 mM NaH_2PO_4, pH 7.4. Likewise, p21A45R, the PR3-resistant p21, was produced as a recombinant His-p21A45R in *E. coli* using the same purification protocol. Because of the presence of the His tag on recombinant p21, the Ala^{45} residue is in position 52. However, we decided to maintain the numbering of wild type p21; therefore, the recombinant PR3-resistant p21 will be called p21A45R in reference to the wild type p21. PR3 was purified from granules of human neutrophils as previously described (21). Silver staining of SDS-PAGE was used to ascertain the purity of p21 and PR3 and to quantify them (data not shown). To perform *in vitro* cleavage, purified recombinant p21 (100 μl) and PR3 (10 μl) (at the indicated concentrations) were incubated in PBS (pH 7.4) at 30 °C for 15 min. After incubation, 5 μl of 10 mM phenylmethylsulfonyl fluoride was added to stop the reaction, and an aliquot of the reaction mixture was run on 15% SDS-PAGE and analyzed by Western blot or by mass spectrometry to visualize the p21 cleavage products.

Matrix-assisted Laser Desorption Ionization Time-of-flight (MALDI-TOF) Mass Spectrometry Analysis

Laser desorption/ionization mass spectrometric analysis was performed with a Perseptive Biosystems (Framingham, MA) Voyager Elite XL time-of-flight mass spectrometer with delayed extraction, operating with a pulsed nitrogen laser at 337 nm (22). Positive ion mass spectra were acquired using a linear, delayed extraction mode with an accelerating potential of 25 kV, a 90% grid potential, a 0.2% guide wire voltage, and a delay time of 200 ns for the recombinant p21 and with an accelerating potential of 20 kV, a 94% grid potential, a 0.15% guide wire voltage, and a delay time of 100 ns for the synthetic p21 peptides (Eurogentec). Each spectrum represents the results from 100 averaged laser pulses. Aliquots (50 μl) of the recombinant p21, treated with PR3 or PBS, were mixed with an equal volume of 1% trifluoroacetic acid (Sigma) and concentrated on a ZipTip™C18 (Millipore Corp.) as specified by the manufacturer. The material eluted was partially evaporated and mixed with an equal volume of a saturated solution of sinapinic acid (Fluka) prepared in a 50% (v/v) solution of acetonitrile/aqueous 0.3% trifluoroacetic acid. Aliquots of 2 μl of this mixture were spotted on the stainless steel sample plate and air-dried prior to analysis. External calibration was performed with myoglobin from horse heart (Sigma) using the *m/z* value of 16,952. Synthetic peptides at a concentration of 12 μM were treated with 10 nM PR3 or PBS as explained in the legends to Figs. 2 and 3. Aliquots of 0.5 μl were mixed with 0.5 μl of a saturated solution of α-cyano-4-hydroxycinnamic acid (Sigma) prepared in a 50% (v/v) solution of acetonitrile/aqueous 0.3% trifluoroacetic acid directly on the stainless steel sample plate and air-dried prior to analysis. External calibration was performed with the calibration mixture 2 of the Sequazyme™ peptide mass standards kit (Applied Biosystems, Foster City, CA) containing angiotensin I (*m/z* 1297.51), fragments of the adrenocorticotropic hormone 1–17 (*m/z* 2,094.46), 18–39 (*m/z* 2,466.72), 7–38 (*m/z* 3,660.19), and bovine insulin (*m/z* 5734.59). The values expressed are average mass and correspond to the $[M + H]^+$ ion.

Molecular Modeling

Preparation of the Starting Structures—The initial set of PR3 coordinates was prepared from the x-ray structure (Protein Data Bank accession number 1fuj (23)) (2.2 Å resolution). Only the 221 residues from chain A of the tetramer were used. Since no structure of the proteinase 3 complexed with a peptide exists, we based our docking strategy on the human neutrophil elastase, its close homologue. We used the x-ray structure (Protein Data Bank code 1PPF) of the complex between human neutrophil elastase and OMTKY3 and the structural similarities between human neutrophil elastase and PR3 to position the peptides in PR3. The geometry of each system was optimized using Charmm (version 30b1) (24) and the Charmm27 force field (25).

Molecular Dynamics Simulations—All MD simulations were run with NAMD (26) and Charmm27, in the (N, P, T) ensemble, using Langevin piston to control the pressure (1 atm) and Langevin dynamics to control the temperature. SHAKE (27, 28) was used to constrain the bond lengths between hydrogen and heavy atoms. Long range electrostatic forces were taken into account using a fast implementation of the particle-mesh Ewald algorithm (29, 30). The equations of motion were integrated using a multiple time step algorithm (31, 32). The systems were initially heated up to 300 K and then stabilized for 100 ps using periodical velocity reassignment and finally simulated for 2000 ps.

Trajectory Analysis—Root mean square deviations of the structures along the simulations were calculated *versus* the initial conformations, in order to check the root mean square stability. We performed an analysis of the last 1.3 ns of the trajectories (sampling time). Average structures of the complexes were calculated over the sampling times, using the Charmm program and subsequently minimized with 2000 steps of steepest descent algorithm and 200 steps of conjugate gradient, solvent molecules being fixed.

Cell Culture, Transfection with Recombinant Plasmids or siRNA, and Differentiation of U937 Cells

U937 cells were cultured in RPMI medium supplemented with 10% FCS and then transfected using the AMAXA system® as indicated by the manufacturer. Briefly, cells (2×10^6) were resuspended in 100 μl of cell line solution in the presence of 1 μg of plasmid (control PRCRSV, PRCRSV/PR3, PRCRSV/p21, or PRCRSV/p21A45R). Cells were electroporated and transferred into culture plates. Transfected cells were selected on the basis on their resistance to neomycin (1 mg/ml) and cloned by limiting dilution. Monocytic differentiation of U937 was performed by adding PMA (Calbiochem) at 62.5 ng/ml. Morphologic analysis was performed using an inverted microscope coupled with a camera. For some experiments, U937 cells were treated with the serine proteinase inhibitor, pefabloc, at 100 μM (Calbiochem) or with the proteasome inhibitor PS-341 (Velcade®, Millennium Pharmaceuticals, Inc., Cambridge, MA) at 0.1 μM. PR3 intracellular expression was assessed by flow cytometry analysis using the mouse monoclonal anti-PR3 (clone CLB-12-8) as the primary antibody followed by a fluorescein isothiocyanate-conjugated anti-mouse antibody using a FACScan flow cytometer (BD Immunocytometry Systems) as previously described (33). The membrane expression of CD11b was measured by flow cytometry after labeling with fluorescein isothiocyanate-conjugated mouse monoclonal anti-CD11b and compared with isotype-specific control IgG (Immunotech, Marseille, France).

For PR3 siRNA experiments, 50 μl of a mix of two PR3-siRNA sequences (Qiagen) (50 nM each) in the presence of Lipofectamine™ at 6.7 μg/ml (Invitrogen) in serum-free Opti-MEM were incubated at room temperature for 30 min to allow the formation of siRNA-liposome complexes. This mix was added to U937 cells previously plated at 3×10^5 in 400 μl of Opti-MEM plus 2% FCS. After 5 h of incubation at 37 °C in a humidified atmosphere with 5% CO_2, FCS-containing RPMI was added in order to obtain a 10% FCS final concentration in 1 ml. Cells were cultured at 37 °C during the indicated period in the presence of siRNA. PR3 target sequences were as follows: TCA GGT GTT TCT GAA CAA CTA and ATC TGT GAT GGC ATC ATC CAA. The silencer negative control 1 siRNA (Ambion) was used to ascertain

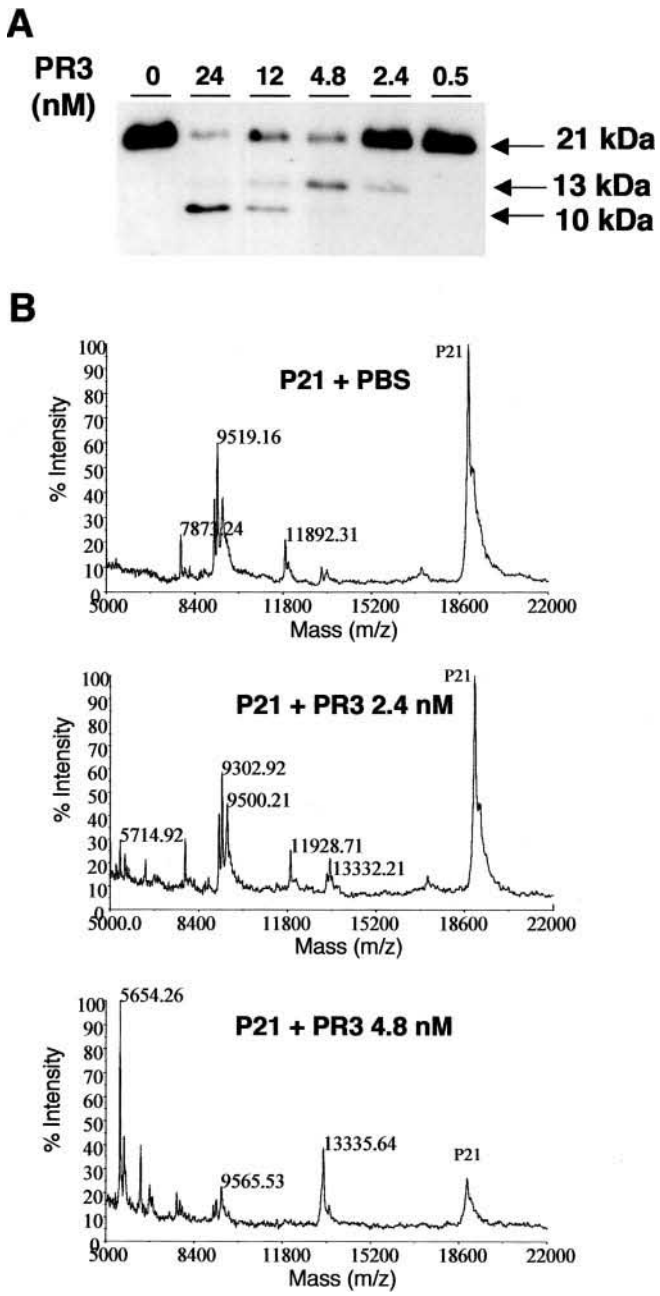

FIG. 1. ***In vitro* analysis of the cleavage fragments of recombinant p21 by PR3.** *A*, Western blot analysis of the cleavage of recombinant p21 by PR3. Recombinant wild type p21 (100 μl at 1.3 μM) was incubated in the presence of neutrophil-purified PR3 (10 μl) at the indicated concentrations at 30 °C for 15 min in PBS at pH 7.4. The reaction was stopped by the addition of 5 μl of 10 mM phenylmethylsulfonyl fluoride. The cleavage samples (20 μl) were mixed with 5 μl of sample buffer and analyzed by SDS-PAGE and Western blot using a polyclonal rabbit anti-p21 directed against a C-terminal epitope on p21. *B*, mass spectra analysis of the p21 fragments by MALDI-TOF. Aliquots (50 μl) of the recombinant p21 treated with PBS or PR3, as indicated above, were mixed with an equal volume of 1% trifluoroacetic acid (Sigma) and concentrated on a ZipTip^{TM}C18 (Millipore Corp.) as specified by the manufacturer. The material eluted was partially evaporated and mixed with an equal volume of a saturated solution of sinapinic acid (Fluka) prepared in a 50% (v/v) solution of acetonitrile/aqueous 0.3% trifluoroacetic acid. Aliquots of 2 μl of this mixture were spotted on the stainless steel sample plate and dried in the air prior to analysis. External calibration was performed with myoglobin from horse heart (Sigma) using the *m/z* value of 16,952.

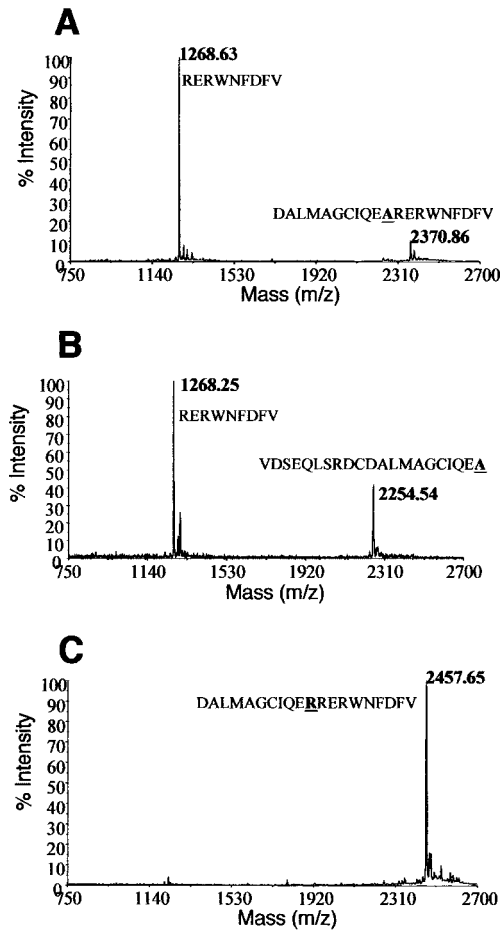

FIG. 2. **Mass spectra analysis of the cleavage of p21 synthetic peptide by PR3 and determination of the amino acid substitution on Ala^{45} to inhibit the cleavage by PR3.** *A*, cleavage of the wild type p21 peptide Asp^{35}–Val^{54}. Wild-type synthetic peptide at a concentration of 12 μM was treated with PR3 at a concentration of 10 nM for 15 min at 30 °C. Aliquots of 0.5 μl were mixed with 0.5 μl of a saturated solution of α-cyano-4-hydroxycinnamic acid (Sigma) prepared in a 50% (v/v) solution of acetonitrile/aqueous 0.3% trifluoroacetic acid directly on the stainless steel sample plate and air-dried prior to analysis. External calibration was performed with the calibration mixture 2 of the Sequazyme^{TM} peptide mass standards kit (Applied Biosystems) containing angiotensin I (*m/z* 1297.51); fragments of the adrenocorticotropic hormone 1–17 (*m/z* 2094.46), 18–39 (*m/z* 2466.72), 7–38 (*m/z* 3660.19); and insulin from bovine (*m/z* 5734.59). *B*, cleavage of the wild type p21 peptide Val^{25}–Val^{54} (as in *A*, except that the synthetic peptide contains an extended N-terminal end and that it was treated for 1 h at 37 °C). *C*, inhibition of the cleavage of the p21 peptide Asp^{35}–Val^{54} containing the A45R mutation.

the specificity of the effect of PR3 siRNA. The Alexa Fluor 488-conjugated negative control siRNA (Qiagen) was used to detect intracellular siRNA by flow cytometry (FL1), thus monitoring the efficiency of transfection after a 2-, 5-, and 18-h incubation period (data not shown).

Cell Cycle and Proliferation Analysis by Flow Cytometry

To carry out a flow cytometry analysis of the DNA content, U937 cells were plated into a 6-well plate (1.5×10^6 cells/ml) in RPMI medium supplemented with 10% FCS with or without PS-341 at 0.1 μM and allowed to seed overnight in culture. The halogenated thymidine analogue bromodeoxyuridine (Pharmingen) at 1 mM was incorporated over 1 h at 37 °C. After resuspension in PBS plus 1% bovine serum albumin, the cells were fixed with frozen 70% ethanol for 18 h at 4 °C. The fixed cells were denatured with 2 N HCl plus 0.5% Triton X-100 during 24 h at 4 °C and then neutralized with 0.1 M $Na_2B_4O_7$ for 30 min. Cells were treated with free RNase-DNase at 300 μg/ml for 1 h at 37 °C, labeled with a monoclonal fluorescein isothiocyanate-conjugated anti-bromodeoxyuridine (Pharmingen) and propidium iodide (Sigma) (2.5 μg/ml) for 30 min at room temperature. Bromodeoxyuridine incorporation (FL1) and propidium iodide (FL2) were analyzed by flow cytometry. Data from 15,000 cells were collected, and the percentages of cells within the G_0/G_1, S, and G_2/M phases of

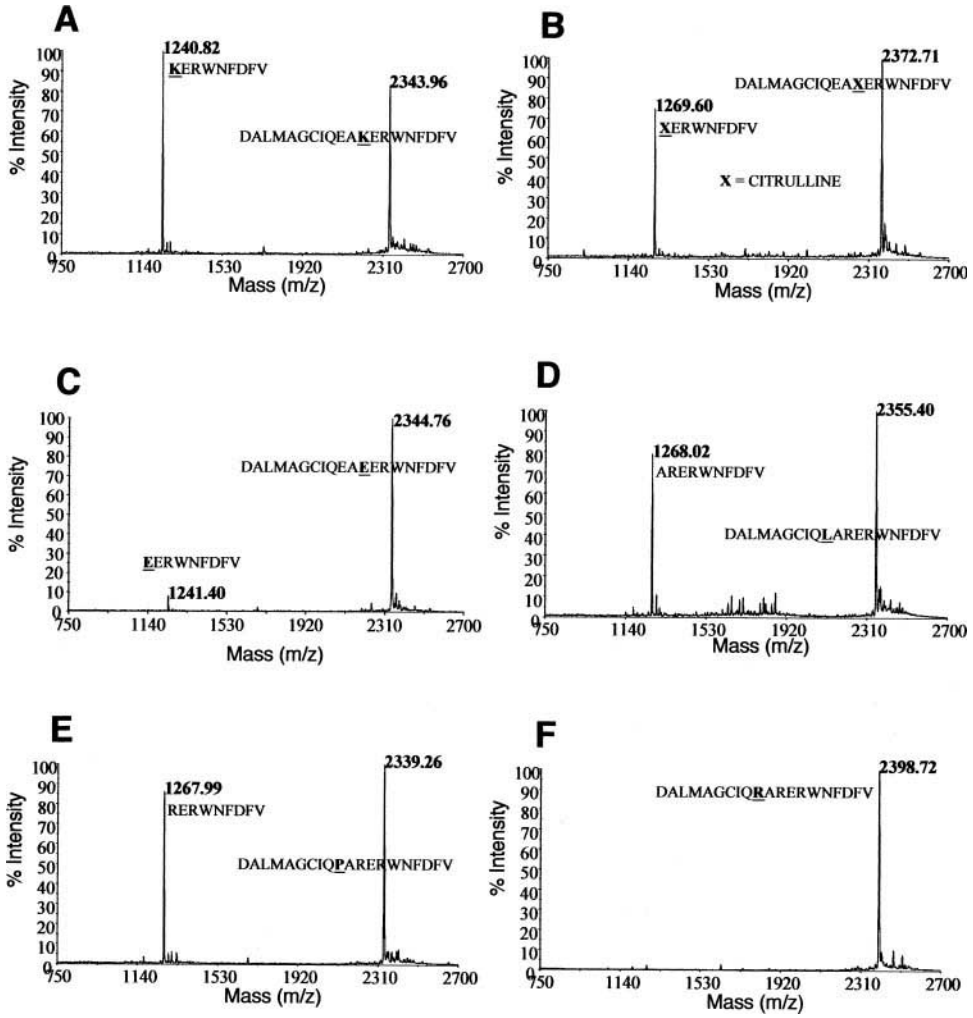

FIG. 3. **Effects of the substitution on the P′1 or P2 sites on the cleavage of p21 peptides by PR3, analyzed by MALDI-TOF.** *A*, cleavage of the synthetic p21 peptide with the P′1 mutation R46K. The p21 peptide (12 μM) was treated with PR3 at a concentration of 10 nM during 15 min at 30 °C. Aliquots of 0.5 μl were mixed with 0.5 μl of a saturated solution of α-cyano-4-hydroxycinnamic acid (Sigma) prepared in a 50% (v/v) solution of acetonitrile/aqueous 0.3% trifluoroacetic acid directly on the stainless steel sample plate and dried in the air prior to analysis. External calibration was performed with the calibration mixture 2 of the Sequazyme™ peptide mass standards kit (Applied Biosystems, Foster City, CA) containing angiotensin I (*m/z* 1297.51), fragments of the adrenocorticotropic hormone 1–17 (*m/z* 2094.46), 18–39 (*m/z* 2466.72), 7–38 (*m/z* 3660.19), and insulin from bovine (*m/z* 5734.59). *B*, cleavage of the synthetic p21 peptide with the P′1 mutation R46Cit (as in *A*, except for the mutation R46*X*, where *X* represents the citrulline). *C*, cleavage of the synthetic p21 peptide with the P′1 mutation in R46E (as in *A*, except that the mutation R46E greatly impaired the cleavage). *D*, cleavage of the synthetic p21 peptide with the P2 mutation in E44L (as in *A*, except for the mutation E44L). *E*, cleavage of the synthetic p21 peptide with the P2 mutation in E44P (as in *A*, except for the mutation E44P). *F*, cleavage of the synthetic p21 peptide with the P2 mutation in E44R (as in *A*, except that the mutation E44R abolished the cleavage).

the cell cycle were determined by Cell Quest (BD Immunocytometry Systems) (34).

Western Blot Analysis

U937 (100×10^6 cells/ml) were lysed into a lysis buffer (0.5% deoxycholate, 0.1% SDS, 1% Nonidet P-40, 150 mM NaCl, 50 mM Tris, pH 8) containing proteinase inhibitors (400 μM aprotinin, 2 mM phenylmethylsulfonyl fluoride, 400 μM leupeptin, 400 μM pepstatin, 2 mM EDTA). Protein concentration was determined using the BCA method (Pierce). Proteins were analyzed by the standard immunoblot procedure as previously described. Rabbit polyclonal anti-p21 (Santa Cruz Biotechnology, Inc., Santa Cruz, CA) or rabbit polyclonal anti-β-actin (Sigma) were the primary antibodies used. The secondary antibody was conjugated with horseradish peroxidase, and the blot was developed using a chemiluminescence detection kit (Amersham Biosciences).

RT-PCR Analysis

Expression of PR3 and p21 mRNA were analyzed by RT-PCR. Total RNA was extracted from U937 cells using SV total RNA isolation System (Promega). After denaturation at 70 °C for 3 min, reverse transcription was performed on 50 ng of total RNA extract at 37 °C for 60 min using Moloney murine leukemia virus reverse transcriptase (Sensiscript; Qiagen). The mRNA of either PR3 or p21 or β_2-microglobulin, which was used as internal control for gene amplification, was amplified by PCR using a GeneAmp PCR System 9600 (PerkinElmer Life Sciences) with the following primers (for PR3, sense (5′-CAC TGC CTG CGG GAC ATA-3′) and antisense (5′-GTC AGG GAA AAG GCG GGT-3′) (35); for p21, sense (5′-GCA TCA CCA CCA CCA CTC AGA-3′) and antisense (5′-CTG TCT TGT ACC CTT GTG CCT CGC-3′); for β_2-microglobulin, sense (5′-CAT CCA GCG TAC TCC AAA GA-3′) and antisense (5′-GAC AAG TCT GAA TGC TCC AC-3′) (36). After denaturation, PCR cycles were conducted as follows: (i) for PR3 and p21, denaturation for 30 s at 94 °C, reannealing for 25 s at 60 °C, and extension for 30 s at 72 °C; for β_2-microglobulin, denaturation for 60 s at 94 °C, reannealing for 60 s at 57 °C, and extension for 120 s at 72 °C; (ii) the number of PCR cycles was determined for PR3 (30 cycles), for p21 (40 cycles), and for β_2-microglobulin (35 cycles) to ensure that quantification of the PCR products was conducted in a linear range of amplification. The PCR products were visualized by electrophoresis in 1% agarose gel containing 0.2 μg/ml ethidium bromide. The β_2-microglobulin gene was used to normalize the PCR products as previously described (36).

Statistical Analysis

Statistical analysis was performed using the Statview™ software package. Comparisons were made by analysis of variance. Differences

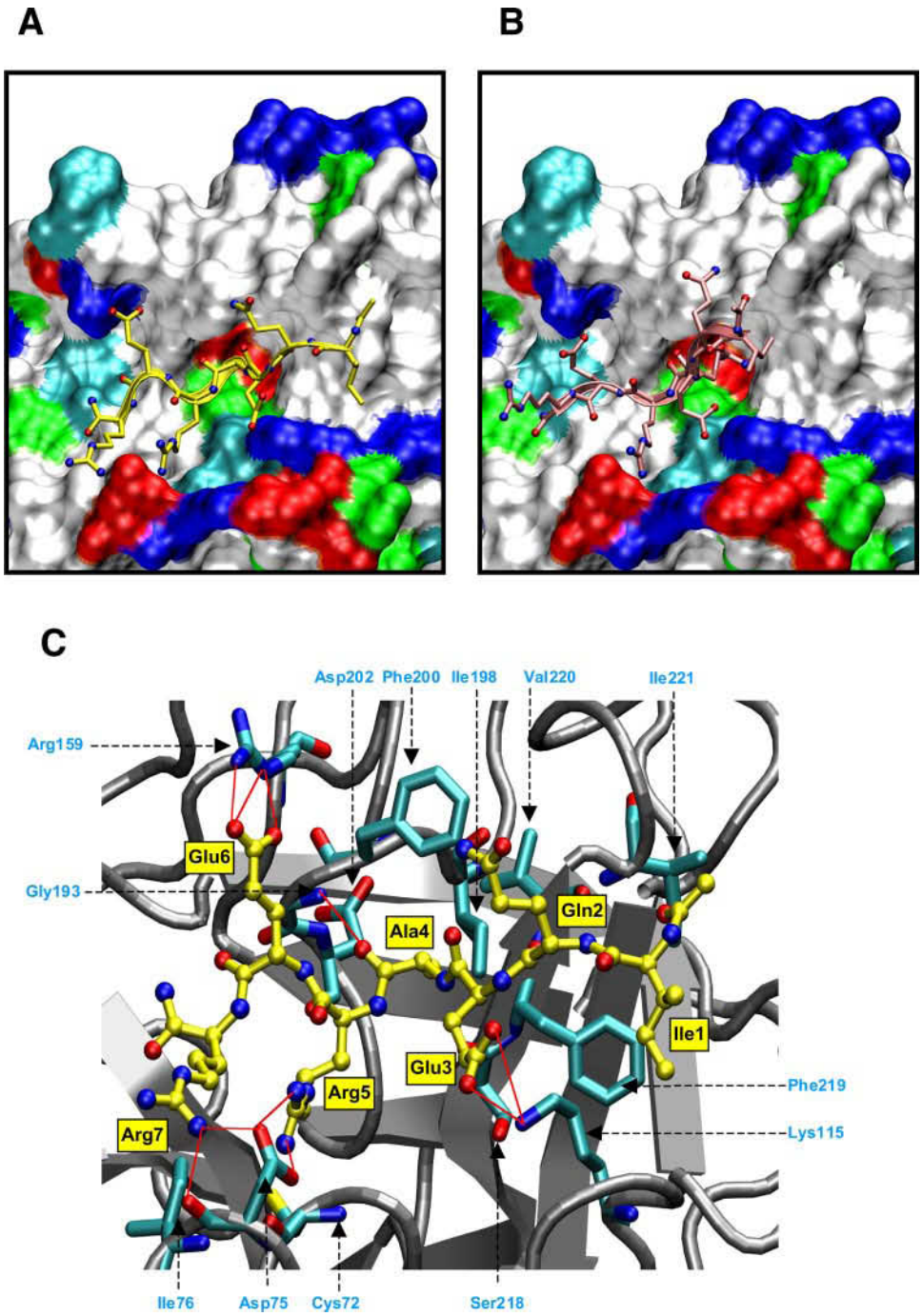

FIG. 4. **Analysis of the complex between PR3 and the p21 peptides by molecular modeling.** *A*, the solvent-accessible surface of PR3 is colored by residue type: *blue* for positively charged residues, *red* for negatively charged residues, *green* for polar, *cyan* for histidines, *white* for hydrophobic residues. pept1 (IQEAER) is drawn using a licorice representation; atoms are *colored* according to their type (*cyan*, carbon; *red*, oxygen; *blue*, nitrogen; *white*, hydrogen). The positively charged residues of the peptide (Arg^5 and Arg^7) interact with negatively charged regions of PR3, whereas negatively charged residues of the peptide (Glu^3 and Glu^6) interact with positively charged regions of PR3. *B*, same as *A* with pept2 (IQERRER) instead of pept1. *C*, residues of PR3 interacting with pept1 are represented with *sticks* (atoms are *colored* by type). The same applies to the peptide, with the exception that its carbon atoms are *yellow*. *Red lines*, as characterized by the MD simulation, represent durable hydrogen bonds.

were considered significant when the p value was less than 0.05 ($p < 0.05$). Data are expressed as mean ± S.E.

RESULTS

Identification of the Specific Cleavage Site by PR3 on p21 by Mass Spectrometry—We previously demonstrated that neutrophil-derived PR3 cleaved recombinant p21 expressed in *E. coli* (12). As shown in Fig. 1*A*, p21 cleavage was dependent on PR3 concentration. Using a rabbit polyclonal anti-p21 antibody directed against a C-terminal epitope, only the carboxyl-terminal fragment could be observed. At low concentration (2.4 nM), the initial p21 fragment had a molecular mass of around 13 kDa. This fragment was further cleaved to a 10-kDa fragment, which we observed at a PR3 concentration of 4.8 nM. The initial cleavage site was identified by mass spectrometry. Mass spectra analysis was performed on purified recombinant p21 with or without PR3. In the absence of PR3, recombinant p21 appeared with a molecular mass of 18,990 Da. In the presence of 2.4 nM PR3, two cleavage fragments at 5714 and at

13,332 Da were observed. These fragments were more apparent at a PR3 concentration of 4.8 nM (Fig. 1*B*). Peptide fragment analysis suggested that the cleavage occurred around Ala^{45} in p21. In order to confirm the cleavage site, a 20-aa p21 peptide (residues Asp^{35}–Val^{54}), DALMAGCIQEA^{45}RERWNFDFV, centered on the P1 residue, Ala^{45}, was analyzed by mass spectrometry with or without the presence of 10 nM PR3. The 20-aa p21 peptide (Asp^{35}–Val^{54}), detected at a molecular mass of 2370 Da, was cleaved and generated a fragment of 1268.63 corresponding to the C-terminal fragment of the peptide after the Ala^{45} position (Fig. 2*A*). Because the N-terminal fragment could not be detected, we hypothesized that the peptide was further cleaved at Ala^{36} or Ala^{39} by PR3. In order to see if Ala^{36} and Ala^{39} could constitute secondary cleavage sites, we performed a trypsin digestion. We were able to observe the presence of the expected N- and C-terminal fragments. We next tested a longer peptide of 30 aa extended at the N terminus. This 30-aa p21 peptide (residues Val^{25}–Val^{54}) was cleaved at Ala^{45} in the presence of PR3. Both the N-terminal and the C-terminal fragments were detected at 2254.54 and 1268.25 Da, respectively, even after 1 h of digestion at 37 °C with 10 nM PR3 (Fig. 2*B*). No cleavage fragment resulting from a cleavage at Ala^{36} or Ala^{39} was observed. Since this synthetic peptide contains two cysteines, which can create a disulfite bond and stabilize it, we also tested a synthetic peptide with a serine in place of the first cysteine. The result was exactly the same (data not shown). Consequently, these results demonstrated that the unique cleavage site, either within the 20-aa or the 30-aa p21 peptide, was on Ala^{45}. In order to determine the mutation on p21, which will render p21 resistant to PR3 cleavage, we analyzed the effect of an arginine substitution, thereby introducing a positively charged amino acid at the P1 position 45 to replace the neutral alanine. Interestingly, the A45R substitution totally abrogated the cleavage of p21 by PR3 (Fig. 2*C*). As previously described, the P1 residue (Ala^{45}) is a small hydrophobic residue. However, the charged amino acids in both P2 and P′1, glutamic acid (Glu^{44}) and arginine (Arg^{46}), respectively, were not classical for PR3. The influence of the charge in the P′1 and in the P2 position was investigated using mutated synthetic p21 peptides centered on Ala^{45}. When the positively charged lysine (Fig. 3*A*) or the neutral citrulline (Fig. 3*B*) were in the P′1 position, the p21 peptide was cleaved. In contrast, when the negatively charged glutamic acid (Fig. 3*C*) was in the P′1 position, the cleavage efficiency was strongly decreased. A similar approach was used to probe the influence of the charge of the amino acid in the P2 position. Cleavage of the 20-aa p21 peptides occurred when the neutral leucine (Fig. 3*D*) or proline (Fig. 3*E*) was in the P2 position. However, the positively charged arginine abrogated the cleavage (Fig. 3*F*). It can therefore be concluded that PR3 can cleave p21 on Ala^{45} with two amino acids of opposite charge in P′1 and in P2. Because the sequence EARER has never been reported in known PR3 substrates, we used molecular modeling to study the conformation of the peptide within the catalytic triad of PR3.

Analysis of the Interaction between p21 Peptide and PR3 Catalytic Triad by Molecular Modeling—To investigate how well the region containing the proposed cleavage site of $p21^{waf1}$ interacts with PR3, we performed MD simulations of a complex between PR3 and a peptide mimicking the cleaved region of p21. As a negative test, we also performed the same simulation on a peptide derived from p21A45R. From the p21 sequence, we chose a peptide centered on the P1 alanine. The sequence contains 3 amino acids before and after the P1 site (alanine 45), since recent studies emphasize the importance of the P′ interaction sites (37) and not only of the P sites (23). The substrate

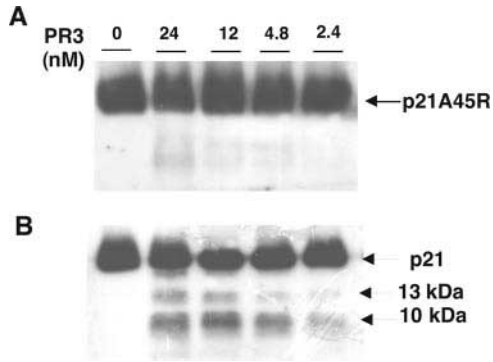

FIG. 5. **Western blot analysis of the cleavage of wild type p21 and the mutated p21A45R by PR3.** Recombinant mutated p21A45R (*A*) and wild type p21 (*B*) were expressed in *E. coli* as a fusion protein expressing an N-terminal His tag. Both recombinant p21s were purified using a nickel affinity column and quantified by SDS-PAGE followed by silver staining. The amounts of p21 and mutated p21A45R were adjusted, and both p21 and p21A45R were incubated with increasing concentrations of PR3 as described in the legend to Fig. 1*A* at 30 °C for 30 min in PBS at pH 7.4. A 40-μl aliquot of the incubation mix was analyzed by Western blot using a polyclonal rabbit anti-p21 directed against a C-terminal epitope on p21. PR3 cleaved wild type p21 in a dose-dependent manner, whereas p21A45R is not cleaved.

sequence docked in PR3 is thus IQE**A**RER (pept1). The trajectories collected during the sampling time were submitted to qualitative and quantitative analysis, including a visual inspection of the trajectories and average structures and calculation of hydrogen bonds and hydrophobic interactions lifetime, respectively. MD simulations results show favorable interactions between amino acids of the peptide and the enzyme. This is illustrated in Fig. 4*A*, where steric and electrostatic complementarities are highlighted. Fig. 4*C* shows persistent hydrogen bonds between peptide and enzyme. In fact, Asp^{202}, Ser^{218}, Arg^{159}, Asp^{75}, and Lys^{115} have previously been reported as important partners in substrate-PR3 interactions (38). The cleavable peptide bond (Ala^4-Arg^5) of pept1 is well positioned in the active site, according to what it should be in a Michaelis complex. The distance between the hydroxyl group of the active serine (Ser^{203}) and the carbon atom of the peptide bond is short and stable. In addition, the CO group of Ala^4 (P1) interacts with the oxyanion hole (NH groups of Ser^{203} and Gly^{201}). Our simulations of the complex between pept1 and PR3 thus reproduce very well the structural properties of a Michaelis complex, suggesting that pept1 is a "good" substrate for PR3.

We performed the same type of calculation for a peptide derived from p21A45R, IQE**R**RER (pept2). We manually docked this peptide into PR3, ran a MD simulation, and analyzed the interactions between the peptide and the enzyme. We found important differences between the two simulated complexes (Fig. 4, *A* and *B*). For the complex with pept2, the distance between the cleavable site and the Ser-OG atom increases along simulation time, indicating that the complex does not resemble a Michaelis complex, which is the "reactant" of the enzymatic reaction. Because of its size, the side chain of arginine creates steric hindrance with PR3, causing structural perturbations of the S1 pocket. Interestingly, the major difference is not only observable for S1/P1. No hydrogen bonds exist between PR3 and residues P4 and P3 (N-terminal side of the peptide) in pept2, unlike for pept1. Moreover, the hydrophobic contacts that existed for the P4 and P3 sites of pept1 and which are an important interaction for substrate specificity and reaction mechanism (38) do not exist with pept2. On the other side of P1 (C-terminal side, after P1), Arg^5 (P′1) has only transient hydrogen bonds with Asp^{75}. The interactions between PR3 (Arg^{159}) and Glu^6 of pept2 are weaker (lower number of hydrogen bonds) than with pept1. We were not able to identify any

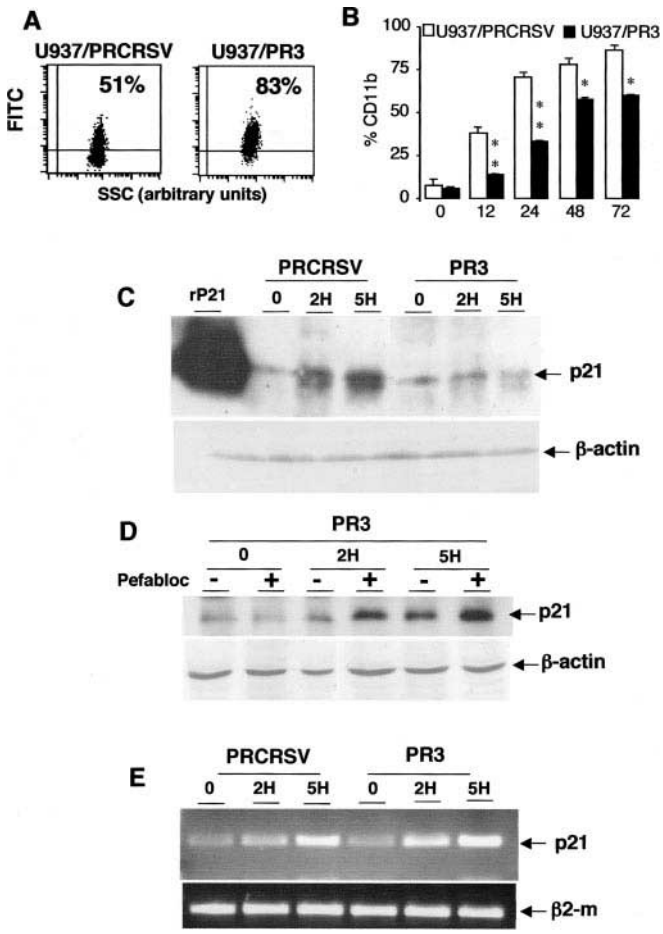

FIG. 6. **Analysis of p21 expression during PMA-induced monocytic differentiation in control U937/PRCRSV and in U937/PR3.** *A*, measurement of intracellular expression of PR3. The intracellular PR3 expression was analyzed by flow cytometry after permeabilization in U937 cells transfected with either the PRCRSV plasmid alone as control (U937/PRCRSV) or the cDNA of PR3 (U937/PR3). PR3 was detected by the monoclonal anti-PR3 (CLB12.8). Labeling with anti-PR3 followed by fluorescein isothiocyanate-conjugated anti-mouse antibody was compared with control IgG1. Ten independent sets of experiments were performed both in U937/PRCRSV and U937/PR3 with a percentage of cells expressing PR3 of 42.2 ± 9.2 and 77.4 ± 10.6%, respectively. The fluorescein isothiocyanate/SSC dot plot depicts the fluorescence and the granulometry, respectively. A representative experiment is shown for U937/PRCRSV and U937/PR3 with 51 and 83% of cells expressing PR3, respectively. *B*, measurement of membrane expression of CD11b during PMA-induced differentiation. Cells were treated with PMA (62.5 ng/ml), harvested at the indicated time, and labeled for CD11b membrane expression, taken as a marker of monocytic differentiation. Results were expressed as the percentage of CD11b-positive cells. Data are mean ± S.E. of 10 independent experiments. A significant decrease was observed in the percentage of CD11b-positive cells in U937/PR3 as compared with U937/PRCRSV ($p < 0.01$ at 12 and 24 h post-PMA and $p < 0.05$ at 48 and 72 h post-PMA). Ten independent sets of experiments were performed both in U937/PRCRSV and U937/PR3. *C*, effect of PMA on p21 expression in U937/PRCRSV and in U937/PR3. Cells were treated with PMA (62.5 ng/ml), harvested at the indicated time, and lysed in lysis buffer supplemented with antiproteinases. A 15% SDS-PAGE was run (100 μg of protein), and Western blot analysis of p21 was performed using a rabbit polyclonal antibody anti-p21 (C-terminal epitope). Recombinant p21 expressed in *E. coli* was used as a positive control (*rp21*; *lane 1*). Expression of p21 was analyzed in the absence of PMA (*0*) and after 2 and 5 h post-PMA treatment for U937/PRCRSV and U937/PR3. Equal protein loading in all wells was checked by measuring the expression of β-actin in the same samples, using a rabbit polyclonal anti-β-actin. Three independent experiments were performed showing the same results, and a representative experiment is shown. *D*, effect of the serine proteinase inhibitor, pefabloc, on PMA-induced p21 expression in U937/PR3. U937/PR3 were preincubated with 100 μM of pefabloc for 24 h before PMA treatment (62.5 ng/ml), and p21 expression was analyzed before (*0*) and after 2 and 5 h post-PMA. In the presence of pefabloc, PR3 was inhibited, and p21 up-regulation in response of PMA could be observed. Three independent experiments were performed showing the same results, and a representative experiment is shown. *E*, effect of PMA on p21 mRNA. U937/PRCRSV or U937/PR3 were cultured for the indicated times (0, 2, or 5 h) in the presence of PMA. The cDNAs obtained after RT-PCR performed on 50 ng of total RNA from U937/PRCRSV or U937/PR3 were used as templates for PCRs using specific primers for p21 or β_2-microglobulin, resulting in the amplification of a 280-bp and a 165-bp fragment, respectively. Before the addition of PMA (*0*), the expression of p21 mRNA was low in both U937/PRCRSV and U937/PR3. A strong up-regulation of p21 mRNA was observed 5 h after PMA in both U937/PRCRSV and U937/PR3. No modulation of the β_2-microglobulin transcripts by PMA was observed. No amplification was obtained in negative controls in the absence of DNA (data not shown). Three independent experiments were performed showing the same results, and a representative experiment is shown.

hydrogen bond between the C-terminal arginine (Arg^7, P4) and PR3. As a result, the tails of the peptide (N- and C-terminal) are solvent-exposed, instead of interacting with PR3, as was the case with pept1 (Fig. 4, *A* and *B*). Our results demonstrate that pept1 forms all necessary interactions with PR3 to be considered a good ligand, whereas pept2 not only has inadequate binding of the P1 residue (Arg), but the whole interaction scheme is perturbed, making the Michaelis complex unstable.

Generation of p21 Resistant to PR3 Cleavage by the Substitution of Ala^{45} for Arg^{45}—In order to validate Ala^{45} as the P1 residue for the initial cleavage of p21 by PR3, a recombinant mutated pETp21A45R was generated by site-directed mutagenesis in *E. coli*. After confirmation of the mutagenesis by direct sequencing, *E. coli* were transformed with pETp21A45R. Recombinant mutated p21A45R was expressed and purified using nickel affinity chromatography. Both wild type p21 and p21A45R were purified from *E. coli* and analyzed by Western blot. Different dilutions of the purified p21 and p21A45R were analyzed by Western blot in order to quantify the initial p21 amount and to load a similar amount in the cleavage assays. Western blot analysis of the cleavage of p21A45R by PR3 showed that it was resistant (Fig. 5*A*), whereas wild type p21 was cleaved by PR3 in a dose-dependent manner (Fig. 5*B*).

It can therefore be concluded that the initial cleavage site of PR3 on p21 was the Ala^{45}. The mutated p21A45R was resistant to *in vitro* PR3 cleavage and thus could be used in a cellular model to investigate the physiological relevance of the specific cleavage of p21 by PR3 in myeloid cells.

Overexpression of PR3 Delayed PMA-induced Monocytic Differentiation and Potentiated p21 Cleavage in U937 Cells—U937 cells were first transfected with either the control plasmid PRCRSV or PRCRSV/PR3 and were selected for 1 month with neomycin. In U937/PR3 that overexpressed PR3, flow cytometry analysis showed a significant increase in intracellular PR3 expression as compared with control U937, which expressed only endogenous PR3 (Fig. 6*A*). PMA was used to induce monocytic differentiation in both control U937/PRCRSV and U937/PR3. The percentage of cells expressing membrane CD11b, taken as a marker of monocytic differentiation, was measured by flow cytometry after 12, 24, 48, and 72 h post-PMA treatment. As shown in Fig. 6*B*, the monocytic differentiation was dramatically delayed in U937/PR3 as compared with control U937/PRCRSV, with $p < 0.01$ at 12 and 24 h post-PMA and $p < 0.05$ at 48 and 72 h post-PMA. Interestingly, the membrane expression of CD11b was correlated with increased cell adherence and clustering of the cells (data not shown). In order to analyze the expression of p21 in U937/PR3 and in control U937 by Western blot, the protein concentration was measured in cell lysates and then adjusted to load 100 μg/well. p21 expression under basal conditions was low in both control U937/PRCRSV and in U937/PR3, and no clear difference was observed (Fig. 6*C*). In U937/PRCRSV,

p21 expression was significantly increased as early as 2 h post-PMA and was further increased after a 5-h PMA treatment. On the contrary, the rapid PMA-induced p21 expression could not be observed in U937/PR3 after a 2- or 5-h PMA treatment. Interestingly, when U937/PR3 were preincubated with the serine proteinase inhibitor, pefabloc, the PMA-induced increase in p21 expression was observed, thereby strongly suggesting that p21 was cleaved by PR3 in U937/PR3 (Fig. 6*D*). Western blot analysis of the β-actin protein on the same membrane was used as an internal loading control to ascertain that the loading was equal in all of the wells (Fig. 6, *C* and *D*). In addition, RT-PCR analysis of p21 mRNA showed that PMA induced a strong transcriptional up-regulation of p21 mRNA in both control U937 and U937/PR3 (Fig. 6*E*). This first set of data showed that the decreased level of p21 expression in U937/PR3, after PMA treatment was the result of its proteolytic cleavage by PR3.

Abrogation of PR3 Activity either by PR3 siRNA or by Ectopic Expression of PR3-resistant p21 Potentiated PMA-induced Monocytic Differentiation in U937 Cells—To determine the function of PR3 in U937 cells, we used the siRNA technology, which results in the specific PR3 inactivation but is not specific for a given protein target of PR3. Successful loss of PR3 mRNA 18 h after one round of siRNA treatment but not a parallel treatment with an irrelevant scrambled siRNA is shown in Fig. 7*A*, using semiquantitative RT-PCR analysis. In contrast, p21 mRNA and β_2-microglobulin mRNA levels were unaffected. Interestingly, immunoblot analysis showed that the amount of p21 protein was increased in U937 cells treated with PR3 siRNA for 18 h as compared with U937 cells treated with scrambled siRNA, thus demonstrating that specific inactivation of PR3 by siRNA resulted in an increased in p21 protein without any variation in the level of p21 mRNA (Fig. 7*B*). To evaluate the role of PR3 on monocytic differentiation, U937 cells were pretreated with either PR3 siRNA or with scrambled siRNA for 7 days after 14 rounds of PR3 siRNA. No effect on cell morphology of either PR3 siRNA- or scrambled siRNA-treated cells was observed in the absence of PMA. In contrast, there was a marked increase in cell adherence and clustering, indicative of a potentiation of monocytic differentiation, in PR3 siRNA-treated U937, 5 h post-PMA treatment (Fig. 7*C*). This effect was not observed in U937 pretreated with scrambled siRNA.

In order to demonstrate that the specific cleavage of p21 by PR3 was functionally linked to the differentiation process, we studied the effect of the ectopic expression of either wild type p21 or the PR3-resistant p21, p21A45R, in U937. U937 cells were transfected with PRCRSV/p21 or with PRCRSV/p21A45R and were selected for 1 month with neomycin. Semiquantitative RT-PCR analysis showed that p21 mRNA expression was clearly increased both in U937/p21 and U937/p21A45R, which express recombinant p21 and endogenous p21, as compared with PRCRSV/U937, which express only endogenous p21 (Fig. 8*A*). Interestingly, there was no difference in the expression of p21 mRNA between U937/p21 and U937/p21A45R. No difference in the amount of β_2-microglobulin mRNA was observed between control U937/PRCRSV, U937/p21, and U937/p21A45R. Under basal conditions, analysis of the cell cycle in U937/p21 and U937/p21A45R showed no difference in G_0/G_1 or in the S phase as compared with the control U937/PRCRSV (Fig. 8*B*). Because the overall p21 proteolytic regulation resulted from the combination of both PR3 and proteasome activities, cell cycle analysis was performed in the presence of PS-341, a selective proteasome inhibitor. As shown in Fig. 8*C*, we witnessed a dramatic decrease in the percentage of cells in S phase in U937/p21A45R treated with PS-341. Interestingly, a significant decrease in the S phase and a concomitant blockade in the G_0-G_1 phase were measured in U937/p21A45R, as compared with U937/p21 or control U937 (Fig. 8*D*). These data suggested that both PR3 and the proteasome participate in the proteolytic regulation of p21 expression in myeloid cells.

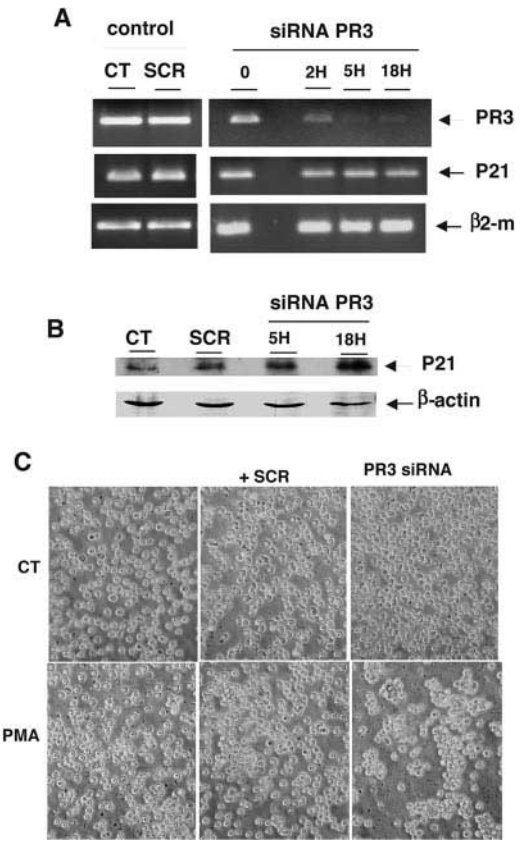

FIG. 7. **Effect of PR3 siRNA on p21 expression and PMA-induced differentiation in U937 cells.** *A*, RT-PCR analysis of PR3 mRNA and p21 mRNA. U937 cells were cultured in the absence (*CT*) or in the presence of scrambled siRNA (*SCR*) used as a negative control or PR3 siRNA for the indicated times (0, 2, 5, or 18 h). The cDNAs obtained after RT-PCR performed on 50 ng total RNA from U937 were used as templates for PCRs using specific primers for PR3 or p21 or β_2-microglobulin. Decreased PR3 transcripts 5 and 18 h after PR3 siRNA treatment of U937 were observed without any modulation of the levels of p21 and β_2-microglobulin mRNA. Three independent experiments were performed showing the same results, and a representative experiment is shown. *B*, effect of PR3 siRNA on p21 protein expression. U937 cells were cultured as described in *A* and were then harvested at the indicated time and lysed in lysis buffer supplemented with antiproteinases. A 15% SDS-PAGE was run (100 μg of protein), and Western blot analysis of p21 was performed using a rabbit polyclonal antibody, anti-p21 (C-terminal epitope). Equal protein loading in all wells was checked by measuring the expression of β-actin in the same samples, using a rabbit polyclonal anti-β-actin incubated with the same membrane. Three independent experiments were performed showing the same results, and a representative experiment is shown. *C*, morphologic analysis of the effect of PR3 siRNA on PMA-induced monocytic differentiation. U937 cells were preincubated for 7 days in the absence or in the presence of control scrambled siRNA (*SCR*) or PR3 siRNA. No clear modification in the morphology of U937 cells could be observed (*CT*; *upper panels*). Cells were then treated with PMA (*lower panels*) at 62.5 ng/ml for 5 h. PMA-induced differentiation was potentiated in U937 cells pretreated with PR3 siRNA as compared with U937 treated with scrambled siRNA. Three independent experiments were performed showing the same results, and a representative experiment is shown.

The influence of the cleavage of p21 by PR3 was evaluated after PMA treatment. Expression of p21 or p21A45R protein was investigated by means of Western blot analysis using a rabbit polyclonal anti-p21 antibody. Under basal conditions, p21 expression was higher in both U937/p21 and U937/

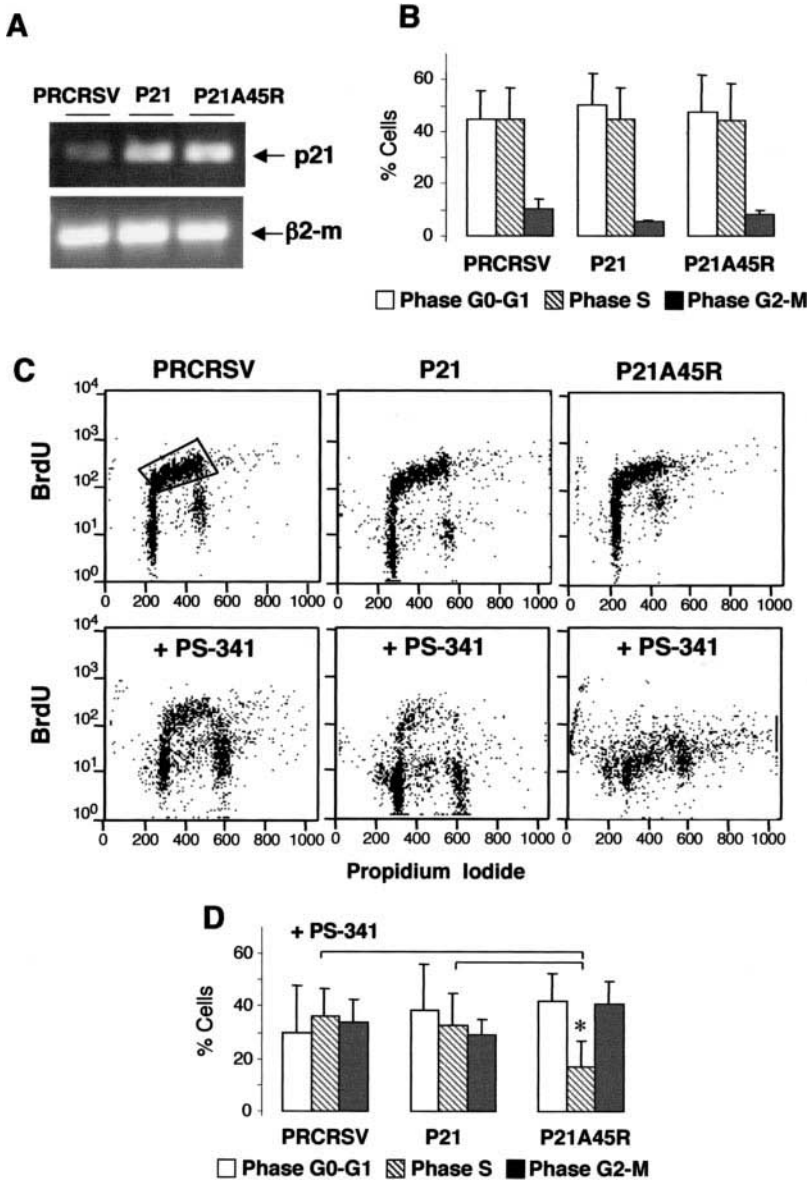

FIG. 8. **Cell cycle analysis by flow cytometry of U937/PRCRSV, U937/p21, and U937/p21A45R.** *A*, RT-PCR analysis of p21 mRNA in control U937/PRCRSV, U937/p21, and U937/p21A45R under basal conditions. The cDNAs, obtained after RT-PCR performed on 50 ng of total RNA from U937/PRCRSV, U937/p21, and U937/p21A45R were used as templates for PCRs using specific primers for p21 or β_2-microglobulin. As expected, the levels of p21 mRNA are stronger in U937/p21 and in U937/p21A45R, which express recombinant p21, as compared with U937/PRCRSV transfected with the empty plasmid PRCRSV. The level of β_2-microglobulin mRNA, used as internal control, was not different between the three cell lines. Three independent experiments were performed showing the same results, and a representative experiment is shown. *B*, cell cycle analysis in basal condition. Cells were analyzed for bromodeoxyuridine incorporation and DNA content. The percentages of cells in the different phases were measured by flow cytometry and analyzed with Cell Quest software. Data are mean ± S.E. of five independent experiments. *C*, representative experiment of the effect of the inhibitor of proteasome PS-341 on the cell cycle in U937/PRCRSV, U937/p21, and U937/p21A45R. U937/PRCRSV, U937/p21, and U937/p21A45R were cultured for 15 h in the presence of 0.1 μM PS-341 before cell cycle analysis. In this representative experiment, the flow cytometry profile showing the percentage of cells in S phase, as indicated by the gate, is as follows: in the absence of PS-341, 48.1, 48.9, and 48.2% for U937/PRCRSV, U937/p21, and U937/p21A45R, respectively; in the presence of PS-341, 24.4, 15.4, and 7.5% for U937/PRCRSV, U937/p21, and U937/p21A45R, respectively. *D*, effect of PS-341 on the cell cycle. Data are mean ± S.E. of four independent experiments. A significant decrease was observed in the percentage of cells in S phase in U937/p21A45R as compared with U937/p21 or U937/PRCRSV ($p < 0.05$).

p21A45R, as compared with control U937/PRCRSV. This was in agreement with the increased expression in p21 mRNA observed in both U937/p21 and U937/p21A45R as compared with control U937/PRCRSV described above (Fig. 8*A*). After a 5-h PMA treatment, differences in p21 expression were more pronounced (Fig. 9*A*). Induction of p21 by PMA was strongest in U937/p21A45R, followed by U937/p21, and was lowest in control U937. After a 24-h PMA treatment, p21 expression was still more in both U937/p21 and U937/p21A45R as compared with the control.

RT-PCR analysis of the PR3 mRNA in PMA-treated U937 demonstrated that PR3 mRNA is abundant in undifferentiated U937 but is significantly lower after a 5-h PMA treatment and cannot be detected after a 24-h PMA treatment (Fig. 9*B*). We observed similar kinetics of PR3 mRNA modulation in U937/p21 and U937/p21A45R. Conversely, the p21 mRNA was strongly up-regulated after PMA treatment in control U937/PRCRSV (already shown in Fig. 6*D*) in U937/p21 and in U937/p21A45. The expression of β_2-microglobulin mRNA was not changed after PMA treatment and was used as an internal control for RT-PCR (Fig. 9*B*). This set of data demonstrated that the involvement of the p21 cleavage by PR3 occurs in the early steps of PMA-induced monocytic differentiation. Interestingly, after a 5-h PMA treatment, the increase in p21 expression observed in U937/p21A45R was concomitant with morphological features of early differentiation (Fig. 9*C*). U937/p21A45R showed the typical morphological changes that occur during differentiation, such as heterogeneous membrane ruffles, cell clusters, and adherence. After a 5-h PMA treatment, these morphological changes were more pronounced in U937/p21A45R as compared with U937/p21, whereas no feature of differentiation was observed in U937/PRCRSV. After a 24-h PMA treatment, there was no obvious difference in the morphology of U937/p21A45R and U937/p21, which both appeared in large clusters. However, there was a clear difference between p21-transfected U937 (both U937/p21 and U937/p21A45R) and the U937/PRCRSV, which showed a less differentiated phenotype.

In conclusion, results from PR3 siRNA experiments, combined with those obtained with ectopic expression of PR3-resistant p21, demonstrated that monocytic differentiation is potentiated when the p21 cleavage by PR3 is abolished.

DISCUSSION

This is the first report that analyzes the physiological implications of PR3 cleavage of p21. Our data demonstrate that in

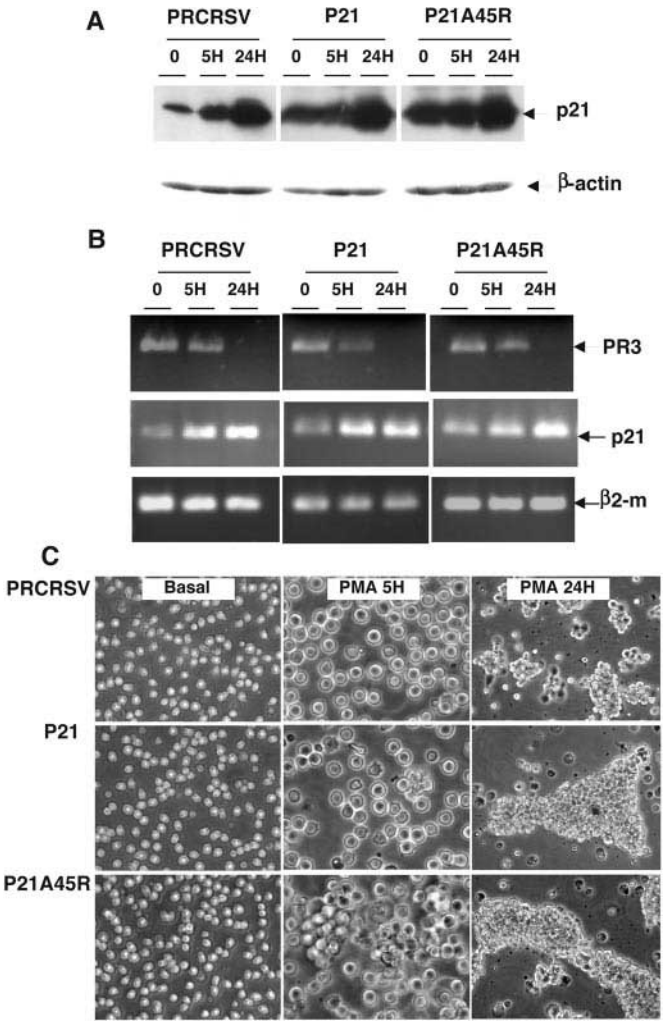

FIG. 9. **Effect of PMA on U937/PRCRSV, U937/p21, and U937/p21A45R.** *A*, Western blot analysis of p21 expression. U937 were treated with PMA (62.5 ng/ml), harvested at the indicated time, and lysed in lysis buffer supplemented with antiproteinases. A 15% SDS-PAGE was run (100 μg of protein), and Western blot analysis of p21 was performed using a rabbit polyclonal antibody, anti-p21. Expression of p21 was analyzed in the absence of PMA (*0*) and after 5 and 24 h post-PMA treatment for U937/PRCRSV, U937/p21, and U937/p21A45R. The expression of β-actin in the same samples was detected, using a rabbit polyclonal anti-β-actin, to validate equal loading of proteins in all wells. Three independent experiments were performed showing the same results, and a representative experiment is shown. *B*, effect of PMA on PR3 mRNA and p21 mRNA. U937/PRCRSV, U937/p21, or U937/p21A45R were cultured for the indicated times (0, 5, or 24 h) in the presence of PMA. The kinetics of the down-regulation of PR3 mRNA levels by PMA was similar in control U937/PRCRSV, U937/p21, or U937/p21A45R. For p21 mRNA, there was an increase in the basal levels of p21 mRNA in U937/p21 and U937/p21A45R as compared with control U937/PRCRSV (as already mentioned in Fig. 8*A*). However, PMA induced a strong up-regulation of p21 mRNA in all three transfectants. No modulation of the mRNA of β_2-microglobulin was observed after PMA treatment. Three independent experiments were performed showing the same results, and a representative experiment is shown. *C*, morphologic analysis of the effect of PMA in U937/PRCRSV, U937/p21, and U937/p21A45R. U937 cells were treated in the absence (basal; *left panel*) or in the presence of PMA for 5 h (*middle panel*) or 24 h (*right panel*) and photographed by phase-contrast microscopy. Under basal conditions, no difference was observed between the three transfectants. In contrast, after 5 h of PMA treatment (*middle panel*), U937/p21A45R showed some typical morphological features of monocytic differentiation with a clear clustering of the cells (*arrow*) and an increased percentage of adherent cells. These features were not observed in U937/p21 or in U937/PRCRSV. After 24 h of PMA treatment (*right panel*), features of monocytic differentiation were more pronounced in U937/p21 and U937/p21A45R than in U937/PRCRSV. Three independent experiments were performed showing the same results, and a representative experiment is shown.

proliferating myeloid precursors, PR3-induced p21 cleavage prevents differentiation. When a stimulus for differentiation occurs, such as PMA, there are two transcriptional events that contribute to cell cycle arrest and subsequent differentiation: the strong induction of the p21 gene and the down-regulation of the PR3 gene. The net result is an increase in p21 protein level because of increased transcription and decreased cleavage. Therefore, it can be concluded that the cleavage of p21 by PR3 is part of the mechanisms that regulate monocytic differentiation. However, there is an alternative interpretation that cannot be ruled out; p21 cleavage by PR3 may prevent cell cycle arrest, which is a critical step before differentiation. Thus, the physiologic function of the p21 cleavage by PR3 might be the modulation of cell cycle rather than direct action on the differentiation process by itself. Differentiation might thus be the default pathway when cells do not cycle and/or do not die.

p21 Cleavage and PR3 Substrate Specificity—Our data demonstrated that the primary site of the cleavage of p21 by PR3 occurred at the Ala^{45} residue. Our data do not agree with a previously reported cleavage site on p21 by PR3, which was on a threonine at 80 in P1, which is a nonclassical P1 site. However, in this study, there was no mass spectrometry and no p21 peptide analyses with mutant studies to confirm this site (39). The preferred PR3 substrates usually contained an Ala in P1 and a hydrophobic residue in P2 and P′1 (40). The cleavage of the Asp^{35}–Val^{54} p21 peptide was inhibited when Ala^{45} was replaced by the positively charged Arg, thereby confirming the preference of PR3 for a small aliphatic amino acid in P1. An analysis of the *in vitro* cleavage by PR3 on the mutant p21A45R expressed in *E. coli* confirmed that p21A45R could not be cleaved by PR3 as compared with the recombinant wild type p21. According to previous work, the preferred P2 and P′1 sites are small aliphatic residues. The cleavage site on Ala^{45} has an unusually large, negatively charged Glu^{44} in P2 and Arg^{46} in the P′1 site. Moreover, our peptide analysis has shown that the p21 cleavage was greatly hampered in the presence of two residues similarly charged in P2 and P1, respectively. Interestingly, molecular dynamics simulations provided compelling evidence demonstrating that the bond between Ala^{45} and Arg^{46} fulfilled the optimal criteria compatible with the cleavage by PR3. According to the previously published structure (23), PR3 can accommodate peptides having a small P1 hydrophobic residue. The other sites also have certain specificities: P4 can be either hydrophobic or polar; P2 can be a polar residue; P′1 and P′3 can be small polar residues; and P′2 can be a polar residue. The IQEARER sequence is unusual because of the P′1 and P′3 residues, which are big polar residues (Arg). Recently, it has been shown that the P′2 residue should be a negatively charged residue (Asp) rather than a proline (41). The results of the molecular dynamics simulations show that the peptide IQEARER forms a valid Michaelis complex, first intermediate of the reaction mechanism of the enzyme. Meanwhile, the hydrogen bond network within the catalytic triad is stable. These results did not reveal any structural characteristics that would be incompatible with the reported cleavage at Ala^{45}. On the contrary, according to our model, the IQERRER containing the A45R substitution has an inadequate binding of the P1 residue, which greatly impairs its cleavage by PR3.

Interaction with Other Functional Sites on p21—Since several distinct functional domains were described within p21, it was important to identify the position of the cleavage site by PR3. The mutation A45R, which was introduced in order to render p21 resistant to PR3 cleavage, is not located within the known interaction domains of p21, such as the cyclin-binding

domain (residues 17–24), the cyclin-dependent kinase 2 binding domain (residues 53–58), and the proliferating cell nuclear antigen-binding domain (residues 144–151) (42, 43). It could therefore be speculated that the mutated p21A45R would have the same binding capacity with its cognate partners. In addition, the p21 cleavage could generate active peptides, still capable of mediating biological functions. It has been recently reported that a small carboxyl-terminal p21 peptide, composed of the residues 139–160 followed by an RYIRS tag, could induce apoptosis (44).

Physiological Relevance of p21 Cleavage by PR3 in Myeloid Cells—The expression of PR3 is restricted to the cells from the myeloid lineage (3). The U937 monocytic or the NB4 granulocytic cell lines expressed endogenous PR3 mRNA, and most of the PR3 is targeted into cytoplasmic granules (19). Monocytic or granulocytic differentiation by PMA or all-*trans*-retinoic acid, respectively, induced down-regulation of PR3 mRNA in HL-60 cells, early in the course of monocytic or granulocytic differentiation (6). In the present study performed in U937 cells, we confirmed the down-regulation of the PR3 gene in the course of PMA-induced monocytic differentiation. Using both gain of function (overexpression of PR3) and loss of function approaches (siRNA and expression of PR3-resistant p21), we provide evidence that the cleavage of p21 by PR3 delayed monocytic differentiation. The corollary is that, when PR3 action is hindered, the system is more reactive. This can be considered as a priming effect or a permissive signal for differentiation or simply a consequence of cell cycle arrest.

Several groups have worked on the expression of p21 induced by PMA in U937 cells. Induction of the p21 promoter in U937 cells by PMA is p53-independent and involves Sp1 binding sites (45). Experiments using antisense p21 have been used to demonstrate the link between the induction of p21 with a G_1 phase cell cycle block after U937 exposure to PMA (46). Several studies support the notion that p21 plays a role in facilitating the monocytic differentiation pathway in U937 (47). In a model of zinc-inducible p21 gene, p21 expression is sufficient, on its own, to induce monocytic differentiation (48). However, in a model of transient expression of p21 (49) or in our model of p21-stably transfected U937, the basal level of p21 expression is not high enough to trigger spontaneous differentiation. The p21 activity can be modulated via transcriptional and post-transcriptional mechanisms as well as by its subcellular localization (50). Transcriptional regulation of p21 is complex and proceeds through multiple pathways including p53-dependent and independent pathways (51). Besides differential phosphorylation, the post-transcriptional regulation of p21 involves its proteolytic cleavage by caspase-3 (52, 53) or its degradation via the proteasome (54, 55), which represents a ubiquitous pathway. It can be concluded from our data (siRNA and p21A45R) that the cleavage of p21 by PR3 is significant and physiologic in a myeloid cell line expressing endogenous PR3. However, the proteolytic regulation of p21 is dependent on both PR3 and the proteasome. In the presence of PS-341 (or bortezomid), an inhibitor of the 26 S proteasome developed as an antineoplastic agent (56), PR3 represent an alternative pathway in the proteolytic regulation of p21.

Acknowledgments—We thank Dr. Noélie Davezac for critically reviewing the manuscript and Romain Chabernaud for skillful technical assistance. Parallab (High Performance Computing Laboratory of the University of Bergen) is thankfully acknowledged for provision of CPU time.

REFERENCES

1. Baggiolini, M., Bretz, U., Dewald, B., and Feigenson, M. E. (1978) *Agents Actions* **8,** 3–10
2. Campanelli, D., Melchior, M., Fu, Y., Nakata, M., Shuman, H., Nathan, C., and Gabay, J. E. (1990) *J. Exp. Med.* **172,** 1709–1715
3. Zimmer, M., Medcalf, R. L., Fink, T. M., Mattmann, C., Lichter, P., and Jenne, D. E. (1992) *Proc. Natl. Acad. Sci. U. S. A.* **89,** 8215–8219
4. Witko-Sarsat, V., Rieu, P., Descamps-Latscha, B., Lesavre, P., and Halbwachs-Mecarelli, L. (2000) *Lab. Invest.* **80,** 617–653
5. van der Geld, Y. M., Limburg, P. C., and Kallenberg, C. G. (2001) *J. Leukocyte Biol.* **69,** 177–190
6. Bories, D., Raynal, M. C., Solomon, D. H., Darzynkiewicz, Z., and Cayre, Y. E. (1989) *Cell* **59,** 959–968
7. Dengler, R., Munstermann, U., al-Batran, S., Hausner, I., Faderl, S., Nerl, C., and Emmerich, B. (1995) *Br. J. Haematol.* **89,** 250–257
8. Molldrem, J. J., Clave, E., Jiang, Y. Z., Mavroudis, D., Raptis, A., Hensel, N., Agarwala, V., and Barrett, A. J. (1997) *Blood* **90,** 2529–2534
9. Lutz, P. G., Moog-Lutz, C., Coumau-Gatbois, E., Kobari, L., Di Gioia, Y., and Cayre, Y. E. (2000) *Proc. Natl. Acad. Sci. U. S. A.* **97,** 1601–1606
10. Rao, J., Zhang, F., Donnelly, R. J., Spector, N. L., and Studzinski, G. P. (1998) *J. Cell. Physiol.* **175,** 121–128
11. Spector, N. L., Hardy, L., Ryan, C., Miller, W. H., Jr., Humes, J. L., Nadler, L. M., and Luedke, E. (1995) *J. Biol. Chem.* **270,** 1003–1006
12. Witko-Sarsat, V., Canteloup, S., Durant, S., Desdouets, C., Chabernaud, R., Lemarchand, P., and Descamps-Latscha, B. (2002) *J. Biol. Chem.* **277,** 47338–47347
13. Sherr, C. J., and Roberts, J. M. (1995) *Genes Dev.* **9,** 1149–1163
14. Gu, Y., Turck, C. W., and Morgan, D. O. (1993) *Nature* **366,** 707–710
15. el-Deiry, W. S., Tokino, T., Velculescu, V. E., Levy, D. B., Parsons, R., Trent, J. M., Lin, D., Mercer, W. E., Kinzler, K. W., and Vogelstein, B. (1993) *Cell* **75,** 817–825
16. Harper, J. W., Adami, G. R., Wei, N., Keyomarsi, K., and Elledge, S. J. (1993) *Cell* **75,** 805–816
17. Steinman, R. A., Hoffman, B., Iro, A., Guillouf, C., Liebermann, D. A., and el-Houseini, M. E. (1994) *Oncogene* **9,** 3389–3396
18. Steinman, R. A., Huang, J., Yaroslavskiy, B., Goff, J. P., Ball, E. D., and Nguyen, A. (1998) *Blood* **91,** 4531–4542
19. Rao, N. V., Rao, G. V., Marshall, B. C., and Hoidal, J. R. (1996) *J. Biol. Chem.* **271,** 2972–2978
20. Waga, S., Hannon, G. J., Beach, D., and Stillman, B. (1994) *Nature* **369,** 574–578
21. Witko-Sarsat, V., Halbwachs-Mecarelli, L., Schuster, A., Nusbaum, P., Ueki, I., Canteloup, S., Lenoir, G., Descamps-Latscha, B., and Nadel, J. A. (1999) *Am. J. Respir. Cell Mol. Biol.* **20,** 729–736
22. Dublet, B., Vernet, T., and van der Rest, M. (1999) *J. Biol. Chem.* **274,** 18909–18915
23. Fujinaga, M., Chernaia, M. M., Halenbeck, R., Koths, K., and James, M. N. (1996) *J. Mol. Biol.* **261,** 267–278
24. Brooks, B. R., Bruccoleri, R. E., Olafson, B. D., States, D. J., Swaminathan, S., and Karplus, M. (1983) *J. Comput. Chem.* **4,** 187–217
25. MacKerell, A. D., Bashford, D., Bellott, M., Dunbrack, R. L., Evanseck, J. D., Field, M. J., Fischer, S., Gao, J., Guo, H., Ha, S., Joseph-McCarthy, D., Kuchnir, L., Kuczera, K., Lau, F. T. K., Mattos, C., Michnick, S., Ngo, T., Nguyen, D. T., Prodhom, B., Reiher, W. E., Roux, B., Schlenkrich, M., Smith, J. C., Stote, R., Straub, J., Watanabe, M., Wiorkiewicz-Kuczera, J., Yin, D., and Karplus, M. (1998) *J. Phys. Chem. B.* **102,** 3586–3616
26. Kalé, L., Skeel, R., Bhandarkar, M., Brunner, R., Gursoy, A., Krawetz, N., Phillips, J., Shinozaki, A., Varadarajan, K., and Schulten, K. (1999) *J. Comp. Phys.* **151,** 283–312
27. Ryckaert, J. P., Ciccotti, G., and Berendsen, H. J. C. (1977) *J. Comp. Phys.* **23,** 327–341
28. Andersen, H. C. (1983) *J. Comput. Phys.* **52,** 24–34
29. Darden, T. A., and Pedersen, L. G. (1993) *Environ. Health Perspect.* **101,** 410–412
30. Essmann, U., Perera, L., Berkowitz, M. L., Darden, T., Lee, H., and Pedersen, L. G. (1995) *J. Chem. Phys.* **103,** 8577–8593
31. Martyna, G. J., Tuckerman, M. E., Tobias, D. J., and Klein, M. L. (1996) *Mol. Phys.* **87,** 1117–1157
32. Izaguirre, J. A., Reich, S., and Skeel, R. D. (1999) *J. Chem. Phys.* **110,** 9853–9864
33. Durant, S., Pederzoli, M., Lepelletier, Y., Canteloup, S., Nusbaum, P., Lesavre, P., and Witko-Sarsat, V. (2004) *J. Leukoc. Biol.* **75,** 87–98
34. Pederzoli, M., Kantari, C., Gausson, V., Moriceau, S., and Witko-Sarsat, V. (2005) *J. Immunol.* **174,** 6381–6390
35. Just, J., Moog-Lutz, C., Houzel-Charavel, A., Canteloup, S., Grimfeld, A., Witko-Sarsat, V., and Cayre, Y. E. (1999) *FEBS Lett.* **457,** 437–440
36. Bauvois, B., Dumont, J., Mathiot, C., and Kolb, J. P. (2002) *Leukemia* **16,** 791–798
37. Korkmaz, B., Attucci, S., Hazouard, E., Ferrandiere, M., Jourdan, M. L., Brillard-Bourdet, M., Juliano, L., and Gauthier, F. (2002) *J. Biol. Chem.* **277,** 39074–39081
38. Hedstrom, L. (2002) *Chem. Rev.* **102,** 4501–4524
39. Pendergraft, W. F., 3rd, Rudolph, E. H., Falk, R. J., Jahn, J. E., Grimmler, M., Hengst, L., Jennette, J. C., and Preston, G. A. (2004) *Kidney Int.* **65,** 75–84
40. Brubaker, M. J., Groutas, W. C., Hoidal, J. R., and Rao, N. V. (1992) *Biochem. Biophys. Res. Commun.* **188,** 1318–1324
41. Korkmaz, B., Attucci, S., Moreau, T., Godat, E., Juliano, L., and Gauthier, F. (2004) *Am. J. Respir. Cell Mol. Biol.* **30,** 801–807
42. Russo, A. A., Jeffrey, P. D., Patten, A. K., Massague, J., and Pavletich, N. P. (1996) *Nature* **382,** 325–331
43. Gulbis, J. M., Kelman, Z., Hurwitz, J., O'Donnell, M., and Kuriyan, J. (1996) *Cell* **87,** 297–306
44. Dong, C., Li, Q., Lyu, S. C., Krensky, A. M., and Clayberger, C. (2005) *Blood* **105,** 1187–1194
45. Biggs, J. R., Kudlow, J. E., and Kraft, A. S. (1996) *J. Biol. Chem.* **271,** 901–906

46. Wang, Z., Su, Z. Z., Fisher, P. B., Wang, S., VanTuyle, G., and Grant, S. (1998) *Exp. Cell Res.* **244,** 105–116
47. Liu, M., Iavarone, A., and Freedman, L. P. (1996) *J. Biol. Chem.* **271,** 31723–31728
48. Asada, M., Yamada, T., Fukumuro, K., and Mizutani, S. (1998) *Leukemia* **12,** 1944–1950
49. Liu, M., Lee, M. H., Cohen, M., Bommakanti, M., and Freedman, L. P. (1996) *Genes Dev.* **10,** 142–153
50. Asada, M., Yamada, T., Ichijo, H., Delia, D., Miyazono, K., Fukumuro, K., and Mizutani, S. (1999) *EMBO J.* **18,** 1223–1234
51. Gartel, A. L., and Tyner, A. L. (1999) *Exp. Cell Res.* **246,** 280–289
52. Gervais, J. L., Seth, P., and Zhang, H. (1998) *J. Biol. Chem.* **273,** 19207–19212
53. Levkau, B., Koyama, H., Raines, E. W., Clurman, B. E., Herren, B., Orth, K., Roberts, J. M., and Ross, R. (1998) *Mol. Cell* **1,** 553–563
54. Maki, C. G., and Howley, P. M. (1997) *Mol. Cell. Biol.* **17,** 355–363
55. Cayrol, C., and Ducommun, B. (1998) *Oncogene* **17,** 2437–2444
56. Adams, J. (2002) *Oncologist* **7,** 9–16